

Surface study of RF magnetron sputtered silicon nitride thin films

U. Majeed^{a,*}, I. Tariq^a, M. Wasib^a, M. K. Mustafa^b

^a*Department of Physics, NED University of Engineering and Technology, Karachi, Pakistan*

^b*Department of Science, Universiti Tun Hussein Onn Malaysia, Pagoh Campus, Johor, Malaysia*

Silicon nitride thin films were deposited on the one-sided P-type polished boron-doped silicon wafer substrate via RF magnetron sputtering using stoichiometric silicon nitride target at various target-to-substrate distances. Target to substrate spacing, a non-conventional parameter, was varied to optimize the surface roughness and grain size. This optimization provided a normal distribution of homogenous, densely packed silicon nitride thin film free of surface cracks. Atomic Force Microscopy was employed to explore the accurate surface roughness parameters of Silicon nitride thin films. The surface roughness and grain analysis for all samples exhibited a direct relation to each other and have an inverse correlation with the target to substrate spacing. The surface morphology of Si₃N₄ was analyzed by the following parameters; average roughness, root-mean square roughness, maximum peak to valley height, ten-point average roughness, skewness, and kurtosis of the line. The surface roughness of silicon nitride films has notable significance in the manufacturing of bio-sensor based on silicon nitride waveguides.

(Received August 4, 2022; Accepted April 3, 2023)

Keywords: Atomic force microscopy, RF magnetron sputtering, Silicon nitride, Target to substrate spacing, Thin film

1. Introduction

Silicon nitride is the most widely used material as dielectric and passivation layer in microelectronics [1] and as structural material in micro-electro-mechanical systems (MEMS), due to its remarkable optical, chemical, and mechanical properties [2, 3]. Silicon nitride thin films also play a vital role in optoelectronics applications due to its high refractive index and transparency in the visible and near-infrared (NIR) region [4, 5]. A major application of silicon nitride thin film in the field of optoelectronics is optical waveguide-based biosensors as a planar optical waveguide [6-8]. A planar optical wave guide is a three-layer structure in which a high refractive index thin film usually called core is sandwiched between two low refractive index films called lower and upper cladding. The optical propagation inside the planar waveguide works on the principle of total internal reflection. It was reported that the roughness of core surface in an optical waveguide is responsible for optical propagation losses at the boundaries of the waveguide [10, 11]. It is due to the phenomenon of reflection and refraction instead of total internal reflection at the interfaces. A rough surface of core could scatter light in different directions. A higher refractive index difference, Δn , between core and cladding promotes the confinement of light in the core. Therefore, a particular structure of silicon dioxide/silicon nitride/silicon dioxide is a suitable candidate for a planar optical wave guide due to refractive index ~ 2 of silicon nitride and silicon dioxide having a refractive index ~ 1.46 as lower and upper cladding creating a refractive index difference $\Delta n \sim 0.5$ [9]. Si₃N₄ thin films are fabricated by low pressure chemical vapor deposition, thermal evaporation, plasma enhanced chemical vapor deposition and magnetron sputtering system [12-16]. However, the Magnetron sputtering technique has considerable advantages over the PECVD technique due to the absence of toxic gases, low temperature deposition, easy to tune deposition rate and simple deposition system [17]. The conventional parameters for thin film

* Corresponding author: uzairmajeed@neduet.edu.pk
<https://doi.org/10.15251/JOBM.2023.152.55>

deposition are sputtering powers [18] and sputtering pressures [19, 20]. However, it is reported that the thin film properties can be varied by altering target to substrate distance while keeping the sputtering power and pressure fixed [21]. Atomic Force Microscopy (AFM) is a magnificent tool to investigate the surface topography on the nanometer (nm) scale [22], including measuring the surface roughness weight, roughness spacing, waviness height, waviness spacing, and lays flaws [23, 24]. Furthermore, AFM is not only used to study surface roughness but also used for bonding, drying, denaturation, and demineralization, etc. [24, 25]. The three-dimensional (3D) topography data can also be used for the further evaluation of surface roughness, average size, and particle size distribution, as well as the porosity of deposited film which directly affects the mechanical, optical, electrical, and surface properties of thin films [26, 27]. In the present work, silicon nitride thin films were deposited on silicon dioxide coated silicon substrates using the RF Magnetron sputtering technique. The aim was to investigate the effect of a non-conventional sputtering parameter i.e. target-to-substrate spacing on surface morphology and the topography of magnetron sputtered silicon nitride thin thin films. The confirmation of formation of amorphous silicon nitride thin films can be found elsewhere [28]. The Atomic force microscopy (AFM) technique was employed to explore the surface properties. The average surface roughness was increased from 0.7nm to ~2nm as the target to substrate distance was reduced from 14 cm to 8 cm. Other statistical surface properties were found to have a nonlinear relationship with target to substrate distance. The packing density of deposited films was found to improve with an increase in target to substrate distance.

2. Material and methods

2.1. Thin film deposition process

One-sided P-type polished boron-doped silicon wafers with 500um thickness and <100> orientation, coated with 1.5um silicon dioxide were used as substrate. All substrates were cleaned in the ultrasonic bath for 10 minutes with acetone and isopropyl alcohol (IPA). After that substrate was washed with deionized (DI) water and dried with industrial grade nitrogen (N₂) gas. Silicon nitride thin films were deposited through the RF magnetron sputtering apparatus (SNTEK, Korea). A stoichiometric (Si₃N₄) circular target (Taewon Scientific, Korea) with a 3" diameter and 1/8" thickness was fixed mechanically to the water-cooled RF electrode. To achieve high purification, the sputtering chamber was evacuated to 4.5×10⁻⁶ Torr using a turbo molecular pump supported with a mechanical rotary pump. Argon (99.99 % pure) was injected in the sputtering chamber with a fixed flow rate of 15 sccm. A pre-sputtering method was employed to purify the sputtering target surface for 3 minutes prior to every deposition. The sputtering process was carried out at constant power 300 W and constant pressure of 5 mTorr. Target to substrate distance was varied as 14 cm, 12 cm, 10 cm and 8 cm to investigate the effect on surface roughness. Samples were rotated constantly at 7 rpm to enhance the film homogeneity. All the trials were conducted without application of external heating to substrate.

2.2. Surface roughness analysis

The characteristics of surface roughness were analyzed by roughness parameters average roughness (R_a), root-mean square roughness (R_q), and maximum peak to valley height (R_t). The surface roughness of Si₃N₄ has notable significance in the manufacturing of microelectronic devices. The topographic scan is run over the sample's surface to probe surface parameters i.e. R_a, R_q, R_t, ten-point average roughness (R_z), skewness of the line (R_{sk}), and kurtosis of the line (R_{ku}). The parameters describing amplitude are the criterion that informs about the heights of a histogram, average values of statistical functions, and some other extreme properties. Ra is the mean value of height which is determined over the whole scanned surface. Ra is ordinarily used to portray the roughness of a fabricated surface of a sample. It is valuable for finding the general deviation in profile height properties and for observing an established assembling process [29]. R_t is the perpendicular distance between the uppermost point of the highest peak and the bottommost point of the lowest valley of the surface which depicts maximum roughness. R_q is the square root of the sum of squares of deviation of height distributions and is viewed as more delicate than the

average roughness for huge deviations from the mean line or plane. The main role of R_q is to calculate the skew and kurtosis parameters and it depicts the optical surface texture. R_z is the vertical height between the mean of five lowest valleys and five highest peaks in the machined surface and is more delicate to infrequent high peaks or low valleys comparatively, Mathematically, R_z is shown by given formulas:

$$R_z = \frac{1}{n} \sum_{i=1}^n (P_i - V_i) \quad (1)$$

The examining points (n) along the appraisal length, which is 5 in this investigation. P_i is the i th peak height of the and V_i is the i th valley depth from the mean line. The abnormality and variations in the profile are calibrated by the R_{sk} . It is a density function of amplitude probability over the surface and is useful to analyze the symmetry of the profile. It helps to explain the resilience, porosity, and attributes of irregular machine measurement. The negative value of skewness is epitomized for a decent bearing profile. Generally, the R_{sk} is used to differentiate between two profiles of equivalent values of R_a and R_q but of distinct textures. Kurtosis is a calculation of spiky points on both sides of the mean line. Kurtosis depicts a machined profile and is utilized for optical characteristics of the surface. It is also determined for the control of fatigue fraction [22]. R_{ku} is used to determine the sharpness of the surface. If $R_{ku} > 3$ the surface has many sharp peaks and valleys, shows a spiky surface and is called leptokurtoic [30]. If $R_{ku} < 3$ the surface has comparatively low peaks and valleys, shows a bumpy surface and is called platykurtoic [30]. The perfect plane surfaces have R_{ku} equivalent to 3. R_{ku} is numerically related to the peak height and valley profundities as per formula:

$$R_{ku} = \frac{1}{NR_a^4} \sum_{i=1}^n Y_i^4 \quad (2)$$

R_{ku} is the RMS roughness parameter and Y_i is the height of the profile at point i .

3. Results and discussion

3.1. Surface roughness

The visualization of the samples is presented by the Park System XEI processing program and surface roughness for each thin film is analyzed by the Gwyddion program. These programs transform the obtained numerical data into visualization and execute different analyses to acquire users' demands. The AFM horizontal scale is set at 3 microns for Si_3N_4 thin film in order to get the better surface texture for optoelectronic applications [28, 29]. The two-dimensional (2D) and 3D AFM images of silicon nitride films at various target to substrate distance i.e., 8 to 14 cm are shown in Figure-1. The decreasing behavior of surface roughness from 1.996 to 0.741 nm was observed by increasing the target to substrate distance from 8 to 14 cm as shown in Table-1.

Table 1. Parameters of surface roughness of silicon nitride thin films deposited at various target to substrate spacing.

No.	Target to Substrate Spacing (cm)	R_a (nm)	R_q (nm)	R_t (nm)	R_z (nm)	R_q/R_a	R_{sk}	Excess Kurtosis	R_{ku}
1	8	1.996	2.483	10.73	7.595	1.243	0.712	0.3127	3.3127
2	10	2.050	2.744	12.6	7.846	1.338	1.326	3.513	6.513
3	12	1.36	1.795	8.025	5.132	1.319	0.987	1.102	4.102
4	14	0.741	0.950	3.724	2.4	1.282	0.387	1.060	4.060

The topographic visualization showing hills and valleys support the above argument as a smoother surface can be observed at higher spacing. As the surface roughness decreases, it is convincing that the larger surface to target distance provides a mean free path and adjustability to Si_3N_4 atoms to settle accordingly on the substrate. The sputtered atoms lose initial energy and direction by colliding gas atoms during the passage and create a uniform growth on the substrate.[33] The target atoms at close spacing have a small mean free path so that sputtered

atoms have less chance to collide with gas atoms and may have higher energy which is responsible for spiky and non-homogeneous grain growth. [34]. It is reported that the growth of grain is responsible for surface roughness. [35].

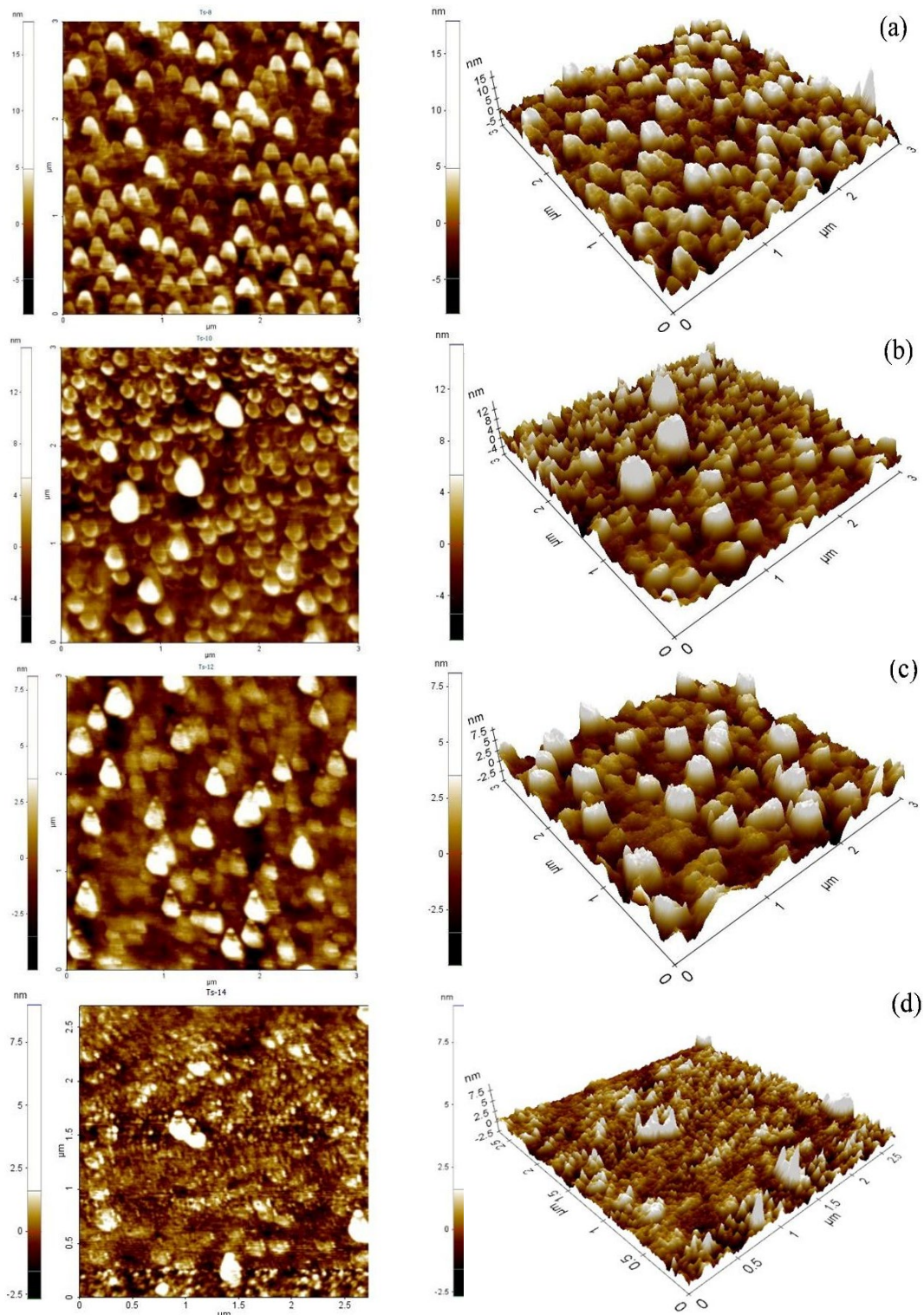
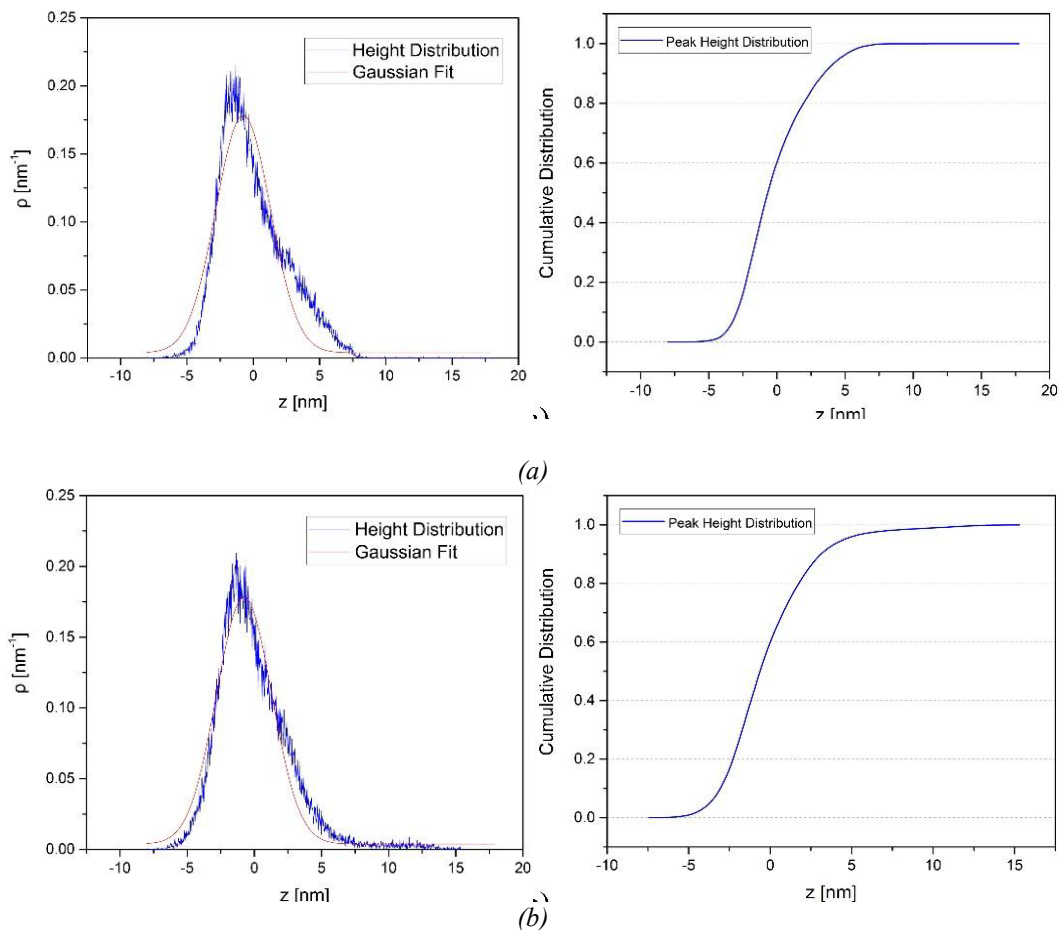


Fig. 1. Silicon nitride thin films 2D and 3D images of at various surface to target spacing, (a) 8cm, (b) 10cm, (c) 12cm, and (d) 14cm.

In Figure-2, the first column shows the histogram for height distribution presenting a statistical representation of probability density function $p[x]$ and the second column is indicating peak height distribution. The height distribution and Gaussian function fit are represented by blue and red lines respectively. The histogram of thin-film produced at 14cm shown in Figure-2(d) is more fit to Gaussian function comparatively, it indicates that this thin film is equally distributed because the measured data near the mean of the plan is more frequent and has uniform roughness. As compare to thin-film composed at 8cm shown in Figure 2(a), the Gaussian function is not fit at the peak and the tail, so that the surface roughness is less normally distributed having uneven peaks comparatively [36]. The trend can be seen in Figure-2(a) to 2(d) when the target to substrate spacing is increased, the graph is attaining more Gaussian normal distribution. The same behavior is observed when the target to substrate spacing increased, the peak height distributions were more normalized.

First column for height distribution histogram and the second for peak height distribution. Table 1 shows the values of roughness parameters R_q and R_z are fluctuating in the same pattern as R_q for all surface to target distances of sputtering to generate Si_3N_4 thin films. The decreasing trend is observed when the surface to target distance is increased after 10 cm. The average roughness at 10 cm is slightly higher than 8 cm but the difference is negligible. Maximum peak to valley height (R_t) is a vital parameter since it reveals the comprehensive roughness of the profile. Table 1 describes the high values of R_t influenced by the high values of R_z because of vertical distance between peak to valley.



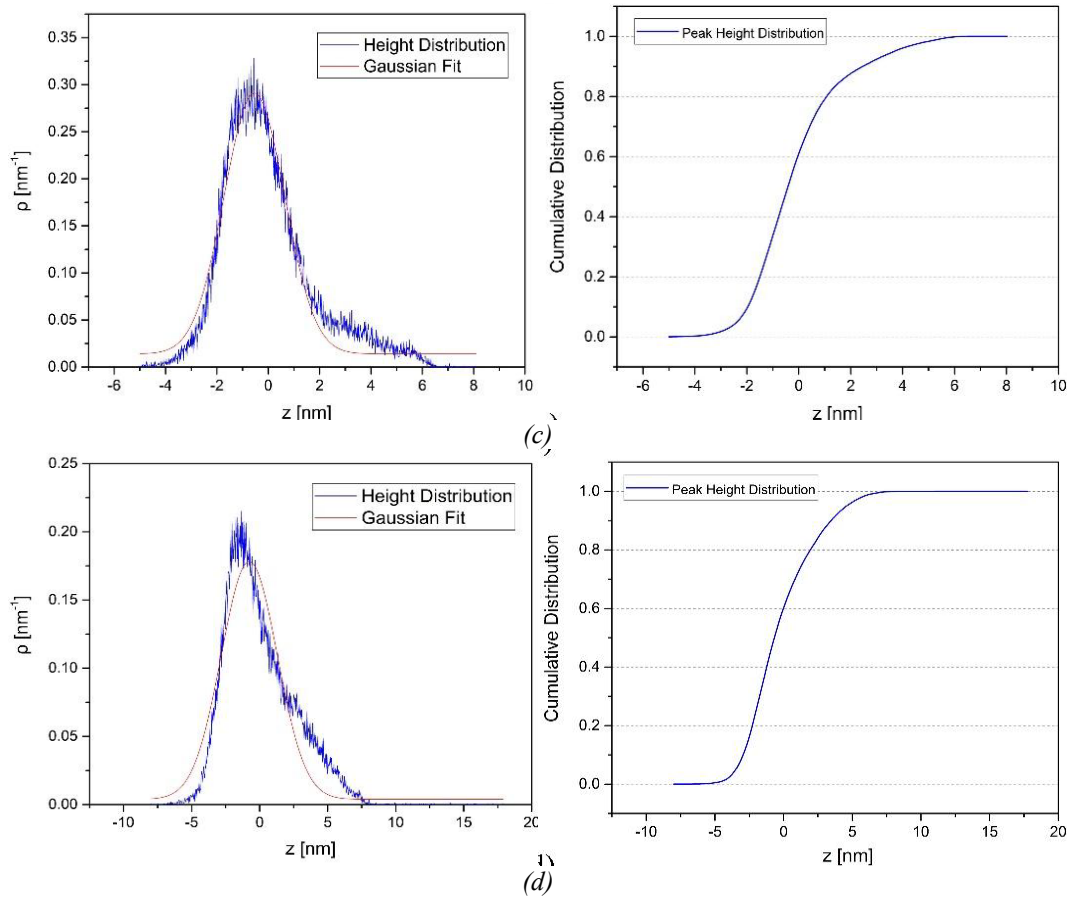


Fig. 2. Surface profile of silicon nitride thin films at a) 8cm, b) 10cm, c) 12cm, and d) 14 cm.

According to the Gaussian distribution of asperity height, the statistical calculations show that the proportion of R_q to R_a must be 1.25. [37] H.C.Ward [38] claimed that the asperity height distribution of most fabricated surfaces might be approached by a Gaussian distribution with the ratio R_q/R_a of approximately 1.31. As demonstrated in Table 1, the statistical values of R_q/R_a measured by AFM scanning are suitable in the range of 1.25 to 1.31 as anticipated by theory. This outcome is notable as it demonstrates that the asperity height distributions of the profile are around Gaussian and the interrelations among roughness parameters are appropriate. The dominant behavior of peaks and valleys over the surface is indicated by positive and negative values of skewness respectively. In Table 1, the continued positive values specify sharpness in the surface responsible for the dominance of peaks. The distribution of both positive and negative values shows the presence of bulged grains. The value of R_{ku} of Silicon Nitrite thin film prepared at 8cm is close to 3, which indicates that the distribution over the examined area has a random surface. The film deposited at 10 cm has a value of R_{ku} more than 6 which shows the highest sharpness and spiky surface. However, the thin films of Si_3N_4 fabricated at 12 cm and 14 cm, the values of R_{ku} are close to 4, the distribution will have moderately higher quantities of high peaks and low valleys with a spiky surface. Films with high R_{ku} values also have high R_t and R_z values. This is because of the solid relation between these parameters.

3.2. Grain analysis

The grain analysis approach depicts a part of the grain ensemble at a predetermined relative level that is shared by all grains. It measures the geometrical parameters of particles in the ensembles. A histogram is used to display a specific geometric characteristic for a portion of grain ensembles.

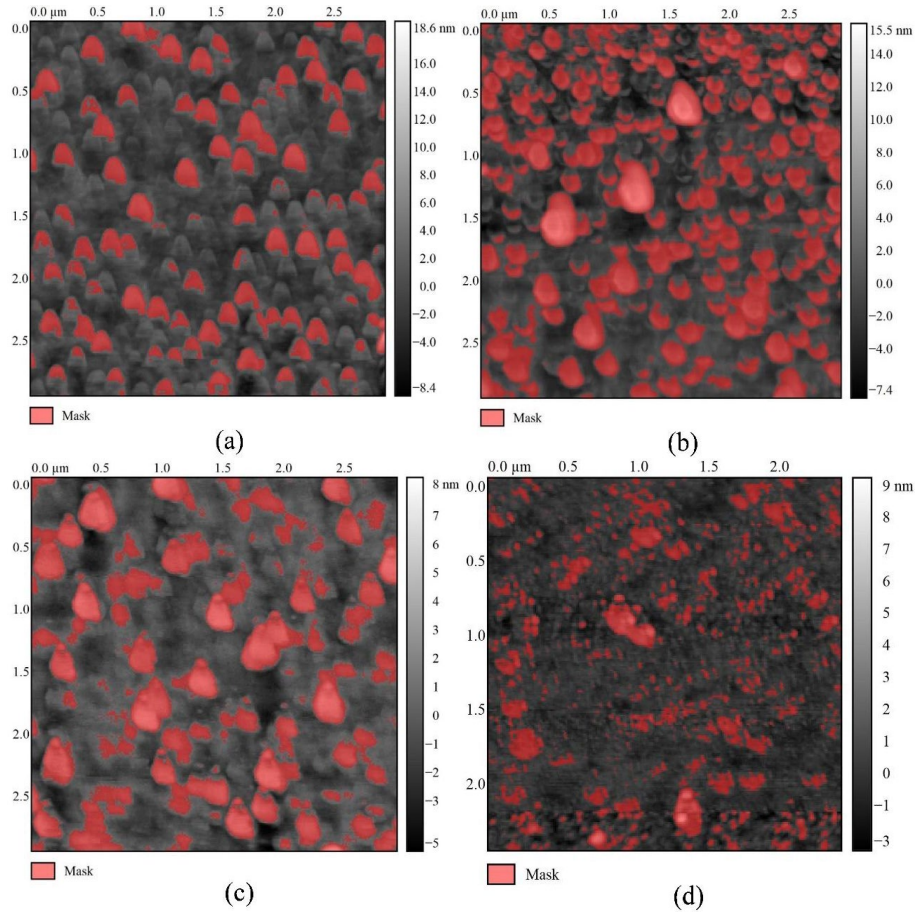


Fig. 3. 2D image shows the grain distribution of Si_3N_4 thin films at various spacing, a) 8cm, b) 10cm, c) 12cm and d) 14 cm.

The images of grain analysis in Figure-3 show a very good distribution of particles all over the surface. The grain analysis approach examines AFM imaging of granular ensembles on the surface based on presupposition, such that the ensemble's particles are positioned on a base surface, their shapes are appropriately convex, and the particles are separated. Statistical measurement can be gathered from a bunch of particles. Furthermore, the most typical statistic measurements are particle counts and distributions of all particle sizes, surface area, and volume. The results are produced using the Gwyddion processing program. Table-2 shows that the increase in target to substrate spacing is responsible for decreasing geometrical characteristics of the surface. It follows the same trend of R_q in Table 1.

Table 2. Geometrical characteristics of grain analysis at the various surface to target spacing.

No.	Target to Substrate Spacing (cm)	Grain Size (nm)	Grain Area (μm^2)	Grain Volume (μm^3)	Grain Perimeter (μm)
1	8	88.38	1.246×10^{-2}	6.658×10^{-3}	0.436
2	10	97.25	1.792×10^{-2}	8.932×10^{-3}	0.559
3	12	72.24	1.394×10^{-2}	5.778×10^{-3}	0.394
4	14	32.27	1.990×10^{-2}	1.214×10^{-3}	0.239

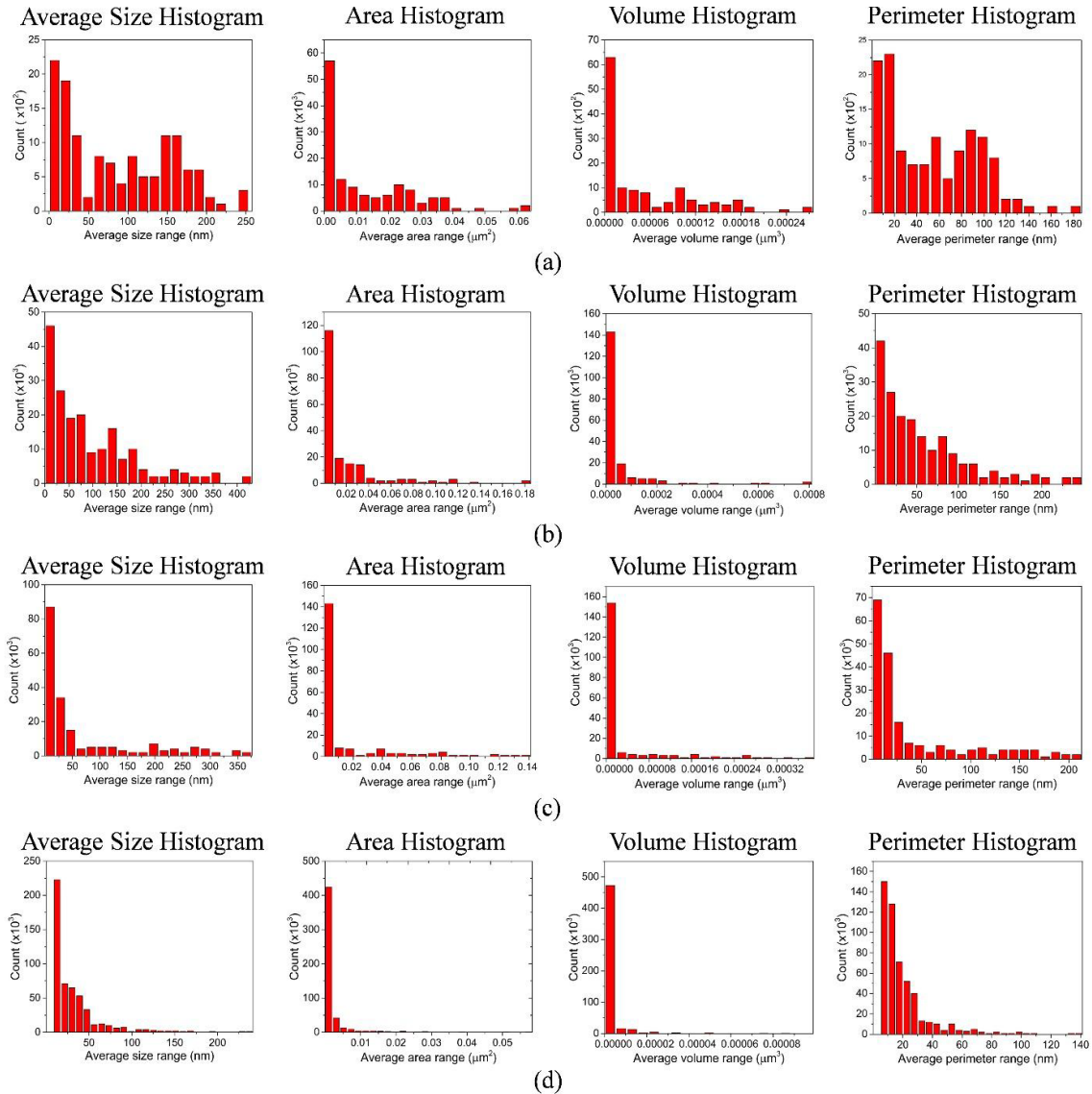


Fig. 4. Quantitative analysis of Silicon nitride thin films at the various surface to target spacing, a) 8cm, b) 10cm, c) 12cm, and d) 14 cm.

The histogram plots of quantitative analysis are shown in Figure-4 also indicate the overall equal distribution of grains on the surface. However, the thin films at the lower target to substrate spacing have a wide range of grain size whereas the histogram plots at higher spacing show the distribution of more equal grain size.

4. Conclusions

Stoichiometric silicon nitride (Si_3N_4) offers higher refractive-index contrast with silicon dioxide (SiO_2) and offers the benefits of increased material stability and high refractive index regularity. This multilayer structure has potential to apply it as optical waveguide-based biosensors.

In this work, Si_3N_4 thin film was deposited on a one-sided P-type polished boron-doped silicon dioxide coated silicon wafer substrate via RF magnetron sputtering at ambient temperature. AFM has been used to study surface roughness and grain analysis. The results of surface roughness and grain analysis are processed by the Gwyddion program. A non-conventional parameter i.e. “target to substrate spacing” was varied to optimize the surface roughness and grain

size. AFM surface profile analysis of all samples revealed normal distribution throughout the surface. The decreasing behavior of surface roughness from 1.996 to 0.741 nm and grain size from 88.38 to 32.27 nm was observed with increasing target to substrate distance from 8 to 14 cm. The topographic visualization of hills and valleys supports the above argument as the smoother surface can be observed at higher spacing. This kind of study could help in adjusting deposition parameters for other materials according to the requirements of surface morphology and to achieve high transparency in the visible region for various applications, such as a bio-sensor based on optical waveguide and integrated circuits in optoelectronics.

Acknowledgments

The authors wish to thank the center for graduate studies, Universiti Tun Hussein Onn Malaysia (UTHM) and Ministry of Higher Education, Malaysia for supporting of this work through FRGS vot 1048. The author also wants to thank Dr. Nafarizal Nayan and staff of MiNT-SRC, UTHM for their valuable guidance and support.

References

- [1] V. Y. Vasiliev, *Journal of Structural Chemistry*, 63(7), 1019, (2022); <https://doi.org/10.1134/S0022476622070022>
- [2] D. Zhou, L. Huang, J. Yuan, and C. Li, *Ceramics International*, 47(22), 32160, (2021); <https://doi.org/10.1016/j.ceramint.2021.08.108>
- [3] K. H. Kim, K. S. Kim, Y. J. Ji, J. E. Kang, and G. Y. Yeom, *Applied Surface Science*, 541, 148313, (2021); <https://doi.org/10.1016/j.apsusc.2020.148313>
- [4] N. Hegedüs, K. Balázs, and C. Balázs, *Materials*, 14(19), 5658, (2021); <https://doi.org/10.3390/ma14195658>
- [5] D. B. Bonneville, J. W. Miller, C. Smyth, P. Mascher, and J. D. B. Bradley, *Applied Sciences*, 11(5), p. 2110, (2021); <https://doi.org/10.3390/app11052110>
- [6] H. Jung, *Current Optics and Photonics*, 3(5), pp. 382-389, (2019).
- [7] A. Nabok, A. M. Al-Jawdah, B. Gémes, E. Takács, and A. Székács, *Toxins*, 13(2), 89, (2021); <https://doi.org/10.3390/toxins13020089>
- [8] A. Nabok, A. Tsargorodskaya, M. K. Mustafa, A. Székács, I. Székács, and N. F. Starodub, *Procedia Chemistry*, 1(1), pp. 1491, (2009); <https://doi.org/10.1016/j.proche.2009.07.372>
- [9] A. V. Nabok, S. Haron, and A. K. Ray, *IEEE Proceedings-Nanobiotechnology* 150(1), (2003); <https://doi.org/10.1049/ip-nbt:20030571>
- [10] H. Kogelnik and T. Tamir, *Guided-wave optoelectronics*, Springer Series in Electronics and Photonics, 26, 57, (1988).
- [11] R. Wu, M. Wang, J. Xu, J. Qi, W. Chu, Z. Fang, J. Zhang, J. Zhou, L. Qiao, Z. Chai, J. Lin, and Y. Cheng, *Nanomaterials*, 8(11), 910, (2018); <https://doi.org/10.3390/nano8110910>
- [12] L. Huang, Z. Ding, J. Yuan, D. Zhou, and Z. Yin, *Ceramics International*, 48(7), 9188, (2022); <https://doi.org/10.1016/j.ceramint.2021.12.104>
- [13] G. Xu, P. Jin, M. Tazawa, and K. Yoshimura, *Thin Solid Films*, 425(1-2), 196, (2003); [https://doi.org/10.1016/S0040-6090\(02\)01089-1](https://doi.org/10.1016/S0040-6090(02)01089-1)
- [14] S. Guruvenket, J. Ghatak, P. Satyam, and G. M. Rao, *Thin Solid Films*, 478(1-2), 256, (2005); <https://doi.org/10.1016/j.tsf.2004.10.031>
- [15] S. Ahn, S. J. Hong, H. S. Yang, and S. M. Cho, *Materials Science in Semiconductor Processing*, 143, 106538, (2022); <https://doi.org/10.1016/j.mssp.2022.106538>
- [16] B.-J. Lee, D.-W. Seo, and J.-W. Choi, *Journal of the Korean Physical Society*, 80(4), 311, (2022); <https://doi.org/10.1007/s40042-021-00354-1>
- [17] M. Signore, A. Sytchkova, D. Dimaio, A. Cappello, and A. Rizzo, *Optical Materials*, 34(4),

- 632, (2012); <https://doi.org/10.1016/j.optmat.2011.09.012>
- [18] U. Majeed, M. K. Mustafa, and N. Nayan, Malaysian Journal of Fundamental and Applied Sciences, 11(2), pp. 52, (2015); <https://doi.org/10.11113/mjfas.v11n2.356>
- [19] H. Zhang, H. Zhu, T. H. Zhang, S. J. Yu, P. C. Guo, Y. X. Wang, & Z. S. Yang, Applied Surface Science, 559, 149968, (2021); <https://doi.org/10.1016/j.apsusc.2021.149968>
- [20] H. Gao, S. Wang, D. Xu, X. Wang, Q. Zhong, Y. Zhong, J. Li, W. Cao, Crystals, 12(1),31, (2022); <https://doi.org/10.3390/cryst12010031>
- [21] N. A. Raship, S. N. M. Tawil, N. Nayan, K. Ismail, M. Tahan, A. S. Bakri, Solid State Phenomena, 317, 471, (2021); <https://doi.org/10.4028/www.scientific.net/SSP.317.471>
- [22] B. R. Kumar and T. S. Rao, Digest Journal of Nanomaterials and Biostructures, 7(4), 1881, (2012).
- [23] C.-E. Morosanu, Thin Solid Films, 65(2), 171, (1980); [https://doi.org/10.1016/0040-6090\(80\)90254-0](https://doi.org/10.1016/0040-6090(80)90254-0)
- [24] F. El Feninat, S. Elouatik, T. Ellis, E. Sacher, and I. Stangel, Applied Surface Science, 183(3-4), 205, (2001); [https://doi.org/10.1016/S0169-4332\(01\)00558-X](https://doi.org/10.1016/S0169-4332(01)00558-X)
- [25] N. Jalili and K. Laxminarayana, Mechatronics, 14(8), 907, (2004); <https://doi.org/10.1016/j.mechatronics.2004.04.005>
- [26] M.H Mamat, A.S Ismail, N. Parimon, N. Vasimalai, M.H. Abdullah, M.F. Malek, M.K. Yaakob, M.K. Ahmad, N. Nafarizal, A.B. Suriani, and A. Mohamad, Materials Chemistry and Physics, 288, 126436. (2022); <https://doi.org/10.1016/j.matchemphys.2022.126436>
- [27] D. Marchetto, A. Rota, L. Calabri, G. Gazzadi, C. Menozzi, and S. Valeri, Wear, 265(5-6), 577, (2008); <https://doi.org/10.1016/j.wear.2007.12.010>
- [28] M. K. Mustafa, U. Majeed, and N. Nayan, ARPN Journal of Engineering and Applied Sciences, 11, 9694, (2016).
- [29] B. Bhushan, Surface roughness analysis and measurement techniques, In Modern tribology handbook, CRC press, 79 (2000); <https://doi.org/10.1201/9780849377877-10>
- [30] N. Kumari, A. K. Singh, and P. Barhai, International journal of thin films science and technology, 3(2), 43, (2014); <https://doi.org/10.12785/ijtfst/030203>
- [31] A. Heredia, C. C. Bui, U. Suter, P. Young, and T. E. Schäffer, Neuroimage, 37(4), 1218, (2007); <https://doi.org/10.1016/j.neuroimage.2007.06.007>
- [32] M. Kwoka, L. Ottaviano, and J. Szuber, Thin Solid Films, 515(23), 8331, (2007); <https://doi.org/10.1016/j.tsf.2007.03.035>
- [33] C. Vasant Kumar and A. Mansingh, Journal of Applied Physics, 65(3), 1270, (1989); <https://doi.org/10.1063/1.343022>
- [34] A. Thaveedetrakul, N. Witit-anun, and V. Boonamnuayvitaya, bioactivity," Applied surface science, 258(7), 2612, (2012); <https://doi.org/10.1016/j.apsusc.2011.10.104>
- [35] M. Wang, J. Wang, W. Chen, Y. Cui, and L. Wang, Materials Chemistry and Physics, 97(2-3), 219, (2006); <https://doi.org/10.1016/j.matchemphys.2005.07.072>
- [36] Y. Chen and W. Huang, Measurement science and technology, 15(10), 2005, (2004); <https://doi.org/10.1088/0957-0233/15/10/010>
- [37] T. King and T. A. Spedding, Wear, 83(1), 91, (1982); [https://doi.org/10.1016/0043-1648\(82\)90343-X](https://doi.org/10.1016/0043-1648(82)90343-X)
- [38] H. Ward and I. Chapter, Profile Characterization. Rough Surfaces, Longman, London, UK, 72, (1982).